Petroleum Science 23 (2026) 2066–2074

Contents lists available at ScienceDirect

Petroleum Science

journal homepage: www.keaipublishing.com/en/journals/petroleum-science

Original Paper

Unveiling the role of Janus nanoparticle shape in trapped oil displacement: A molecular perspective

Yuan-Hao Chang [a,b], Rui Ma [b], Bo Wang [c,d], Han-Zhou Li [d], Fan-Hua Zeng [c,*], Jian-Ying He [b,**]

[a] School of Petroleum Engineering, Xi'an Shiyou University, Xi'an, 710065, Shaanxi, China
[b] Department of Structural Engineering, Norwegian University of Science and Technology (NTNU), 7491, Trondheim, Norway
[c] Petroleum Systems Engineering, University of Regina, Regina, Saskatchewan, S4S 0A2, Canada
[d] Sinopec Jiangsu Oilfield Company, Yangzhou, 225009, Jiangsu, China

ARTICLE INFO

Article history:
Received 20 June 2025
Received in revised form
12 December 2025
Accepted 15 December 2025
Available online 17 December 2025

Edited by Yan-Hua Sun

Keywords:
Janus nanoparticles
Enhanced oil recovery
Molecular dynamics simulation
Shape of nanoparticle
Wettability alteration

ABSTRACT

Janus nanoparticles (JNPs) exhibit significant promise for enhancing oil recovery (EOR). However, their large-scale field deployment remains challenging. A key challenge lies in the insufficient understanding of how the physical characteristics of JNPs influence their transport behavior and microscopic oil displacement mechanisms in porous media. In this study, molecular dynamics (MD) simulations are employed to systematically investigate the displacement dynamics of oil trapped on rough surfaces mediated by JNPs of various geometries. The results reveal that particle shape critically affects both the pinning resistance encountered at groove edges and the accumulation patterns along lateral walls. These shape-dependent adsorption configurations in turn modulate local wettability and ultimately dictate the efficiency of oil removal from nanoscale grooves. Spherical and ellipsoidal JNPs demonstrate superior displacement performance when the groove surface is coated with a thin oil film. However, under conditions involving thick oil films, spherical JNPs exhibit limited penetration into narrow grooves due to their stable orientation at the oil–water interface, which reflects strong interfacial stability. In contrast, disc, rod, and ellipsoidal JNPs effectively disrupt thick oil films via a cooperative mechanism termed "aggregation and flipping". Among all evaluated geometries, ellipsoidal JNPs consistently deliver optimal EOR performance across various oil film conditions. These findings provide molecular-level insights into shape-governed JNP performance in EOR, offering valuable guidance for the rational design and application of shape-optimized JNPs in oilfield operations.
© 2025 The Authors. Publishing services by Elsevier B.V. on behalf of KeAi Communications Co. Ltd. This is an open access article under the CC BY license (http://creativecommons.org/licenses/by/4.0/).

1. Introduction

In recent years, despite the rapid growth of renewable energy, fossil fuels still maintain their dominant position, accounting for over 80% of the global energy supply. Projections indicate that global demand for fossil fuels is expected to increase by more than 30% within the next 20 years (Newell et al., 2019). Given the increasing challenges associated with exploring and developing new oil fields, it is imperative to implement enhanced oil recovery (EOR) techniques in existing fields to meet the demand for petroleum consumption (Bai, 2008; Lyons and Plisga, 2011; Richards et al., 1996). However, conventional EOR methods currently face obstacles such as high energy and chemical costs, gravity override, fingering, early breakthrough, and formation damage (Ahmadi et al., 2015; Olajire, 2014; Sun et al., 2015).

To address these challenges, nanoparticles (NPs) have emerged as a promising solution due to their small size, high surface area-to-volume ratio, cost-effectiveness, and environmental compatibility (Almahfood and Bai, 2018; Haruna et al., 2020; Sun et al., 2017). Particularly, Janus nanoparticles (JNPs) with distinct wetting properties on their surfaces have gained increasing attention for their application in EOR (Jia et al., 2021b; Shi et al., 2019; Wu et al., 2020b). Encouraging findings have revealed that JNPs hold tremendous potential for improving the interface and rheological parameters within the

* Corresponding author.
** Corresponding author.
E-mail addresses: fanhua.zeng@uregina.ca (F.-H. Zeng), jianying.he@ntnu.no (J.-Y. He).
Peer review under the responsibility of China University of Petroleum (Beijing).

https://doi.org/10.1016/j.petsci.2025.12.024
1995-8226/© 2025 The Authors. Publishing services by Elsevier B.V. on behalf of KeAi Communications Co. Ltd. This is an open access article under the CC BY license (http://creativecommons.org/licenses/by/4.0/).

oil–water–rock system during the EOR process, surpassing the performance of traditional homogeneous NPs (Gao et al., 2025; Liu et al., 2025; Tang et al., 2024; Wu et al., 2024; Zang et al., 2024). Specifically, Giraldo et al. (2019) observed that the NiO/SiO_2 Janus nanofluid exhibited significantly higher viscosity compared to the SiO_2 nanofluid. This enhancement can be attributed to the attractive binding energy of NiO within the structure of the NiO/SiO_2 JNPs, which promotes increased particle adhesion. Additionally, the reduction of interfacial tension (IFT) and alteration of surface wettability have long been recognized as pivotal factors for nanofluids in EOR (Chang et al., 2022). In this regard, JNPs have proven to be more effective than conventional homogeneous NPs in reducing IFT and altering the wettability of rock surfaces, owing to their amphiphilic structures (Betancur et al., 2016; Rosales et al., 2006; Tohidi et al., 2022). Furthermore, Luo et al. (2016) focused on graphene-based Janus nanosheets, revealing two distinct oil displacement mechanisms associated with Janus nanosheets: the climbing film growth mechanism and the slug-like displacement mechanism.

Despite the evident promise of JNPs in EOR, their extensive implementation in field applications remains a significant challenge (Tohidi et al., 2022). One significant reason for this is the intricate and substantial impact of the diverse physical properties of JNPs on their performance in reservoirs. Among the various types of JNPs, modified MoS_2 exhibited the greatest reduction in IFT (Raj et al., 2019), while graphene-based amphiphilic nanosheets showed the largest alteration in oil contact angle (Rosales et al., 2006). Furthermore, the concentration of JNPs has vital effects on their interfacial behavior. For instance, higher concentrations of SiO_2-C_{12} JNPs led to lower interfacial tension (Wu et al., 2020a). Also, increasing the concentration of Janus-C_{12} resulted in enhanced emulsion stability and a remarkable reduction in droplet size (Jia et al., 2021a). This improved stability can be attributed to the formation of denser interfacial membranes that prevent droplet coalescence at higher Janus-C_{12} concentrations (79%). Moreover, although studies have confirmed that NPs of various shapes exhibit notable EOR performance, comprehensive comparative investigations under identical fluid-rock systems remain lacking (Aadland et al., 2020; Geng et al., 2024; Hu et al., 2016; Zang et al., 2024). In fact, experimental results have shown that transitioning from spherical to sheet-like structures can enhance dispersibility, lower interfacial tension, and improve displacement efficiency (Zaid et al., 2014). Simulations further suggest that while spherical JNPs tend to maintain a consistent average orientation at the oil–water interface regardless of their surface properties or densities, the behavior of ellipsoidal JNPs is significantly influenced by these factors, thereby altering their interfacial alignment (Luu and Striolo, 2014). These findings collectively imply that JNP shape governs their interactions within fluid–rock environments, ultimately leading to distinct displacement mechanisms and EOR outcomes. Therefore, systematic investigations are urgently needed to delineate the shape-dependent adaptability of JNPs within specific reservoir conditions.

Herein, molecular dynamics (MD) simulations are employed to explore the impact of JNP shape on trapped-oil displacement. Specifically, the oil recovery efficiency of JNPs with various shapes is presented. The differences in detailed motion characteristics of these JNPs, including their anchoring onto the solid surface, entry into oil trapping grooves, and alteration of local surface wettability, are elaborated upon. Furthermore, the influence of oil film thickness is discussed. The findings of this study shed light on the mechanisms by which JNPs of different shapes facilitate the trapped oil recovery, thereby aiding in the design and application of JNPs in EOR.

2. Model and simulation details

The LAMMPS package is utilized for all MD simulations in this study (Plimpton, 1995). Visualization and analysis are conducted using the OVITO software (Stukowski, 2009). As shown in Fig. 1, an atomic system is constructed to capture the crucial characteristics of oil trapped on the rough surface. The system possesses periodic boundaries and consists of residual trapped oil and nanofluids. The grooved surface, namely the nanogroove with dimensions of 102.7 × 71.7 × 50.5 $Å^3$, is created by removing the atoms from the solid substrate composed of silicon crystals. To mitigate periodic effects, the surface height at the thinnest region of the groove is set to 11 Å, surpassing the cutoff distance of 10 Å. Hexane molecules are absorbed on the solid surface and in the nanogroove to mimic the residual trapped oil remaining after initial water flooding, with an oil density matching experimental conditions. The thickness of the oil film on the flat surface in the reference group is 5 Å, which will further be adjusted to 10 and 15 Å in the subsequent sensitivity study (as shown in the bottom left section of Fig. 1). For the flooding phase, 48 silicon JNPs and approximately 21,000 water molecules are employed to construct the nanofluid. As the focal point of the study, JNPs are respectively designed in shapes including spherical, rod, ellipsoidal, and disc forms within the system (as displayed in the top left section of Fig. 1). JNPs of various shapes are constructed based on a silicon crystal lattice, in which atoms were selectively removed through programmed calculations to obtain the desired geometries. The volume of individual JNPs with different shapes is kept nearly identical at approximately 520 $Å^3$ for comparison. Specifically, the rod-shaped nanoparticles have a length of 22.7 Å and a diameter of 5.4 Å; the disk-shaped nanoparticles exhibit a thickness of 1.9 Å and a diameter of 9.3 Å; while the ellipsoidal nanoparticles possess semi-axis lengths of 3.5, 3.5, and 10.2 Å along the three principal axes, respectively. As the JNPs are designed to have identical volumes to ensure comparable mass and material content, the surface areas inevitably vary with particle geometry.

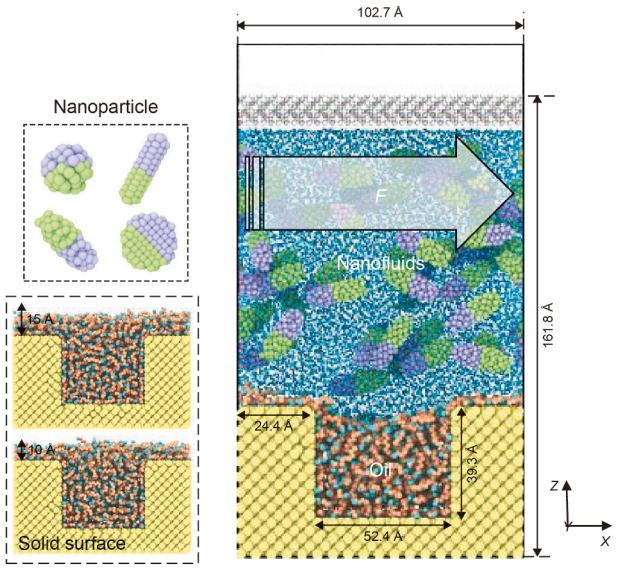

Fig. 1. Schematic of the simulation system. The grey arrow indicates the displacement direction. The colors for different components: water (light blue), methylene (orange), methyl (cyan), surface (light yellow), hydrophobic part (light purple), and the hydrophilic part (light green) of JNP. The color scheme applies to all snapshots in the following figures unless otherwise specified.

In the systems, the monoatomic water (mW) model is employed to represent water molecules, while the transferable potentials for phase equilibria united-atom (TraPPE-UA) description of hexane is chosen for modeling oil molecules. Specifically, the mW model incorporates the Stillinger–Weber (SW) potential to account for many-body non-bonded interactions (Molinero and Moore, 2009), while the non-bonded interactions between water–oil and oil–oil utilize the standard pairwise 12-6 Lennard–Jones (LJ) potential (Martin and Siepmann, 1998). To highlight the hydrophobic nature of the rock surface in the residual oil-enriched region, the characteristic energy ε_{ws} (water-surface) is set as 0.3 kcal/mol (Chang et al., 2021). The characteristic energy for interactions involving JNPs is determined based on previous studies (Wang et al., 2019, 2020).

During the simulations, the systems undergo an initial energy minimization using the steepest descent method, followed by a 2 ns equilibrium stage in the NVT ensemble at 353 K. To maintain the desired temperature, the Nosé–Hoover thermostat with a coupling coefficient of 100 fs is employed (Hoover, 1985; Nosé, 1984). Another 90 ns non-equilibrium MD simulation (NEMD) is then conducted for each system, to mimic the nanofluid flooding process. A constant force (0.007 kcal/(mol·Å)) along the *X*-axis is applied to each water molecule. Besides, to improve simulation efficiency, the JNPs are treated as rigid bodies, and the rough surface is kept fixed in position. Five independent simulations are performed for each system to enhance the statistical robustness of the results.

3. Results and discussion

3.1. Displacement of residual oil in nanogrooves

The incorporation of JNPs with different shapes into the flooding significantly influences the displacement of the trapped oil in the nanogroove. As shown in snapshots after simulation (Fig. 2(a)), JNPs actively interact with both the solid substrate and the trapped oil, adsorbing onto the rough surface and penetrating one side of the oil-filled groove. Moreover, the adsorption dynamics of JNPs along the lateral walls vary significantly with particle shape, as detailed in Fig. S1. Spherical and ellipsoidal JNPs exhibit a gradual accumulation process, progressing from the groove edge toward the interior. In contrast, rod and disc JNPs rapidly establish stable adsorption configurations, forming bilayer and monolayer adsorption films, respectively. Besides, all JNPs adsorbed on the inner wall of the groove orient their polar ends in the direction of flow, facilitating water intrusion and subsequent oil displacement.

These distinct adsorption behavior leads to varying amounts of residual oil after displacement. The EOR effect in the nanogroove is defined as the percentage of oil molecules displaced out of the groove at the end of the simulation. As depicted in Fig. 2(b), spherical and ellipsoidal JNPs hold the most pronounced oil displacement effects, with a recovery rate exceeding 40%. Rod JNPs achieve an EOR of approximately 33%, while disc JNPs demonstrate a much lower EOR, around 20%. This poor displacement performance of disc-shaped JNPs for thin film-like residual oil contrasts with previous experimental studies where nanosheets exhibited superior performance in generating structural disjoining pressure and stabilizing foams. This discrepancy further underscores the necessity for more refined investigations into the shape-dependent EOR mechanisms and application-specific suitability of nanoparticles. Furthermore, the distribution of residual oil inside the groove after displacement elucidates the displacement effects affected by JNP shapes. According to Fig. 2(c), on the side of the groove where JNPs accumulate, rod-shaped JNPs retain more residual oil whereas spherical JNPs result in the least amount of remaining oil molecules. This variation is attributed to differences in the surface coverage area of the nonpolar domains among

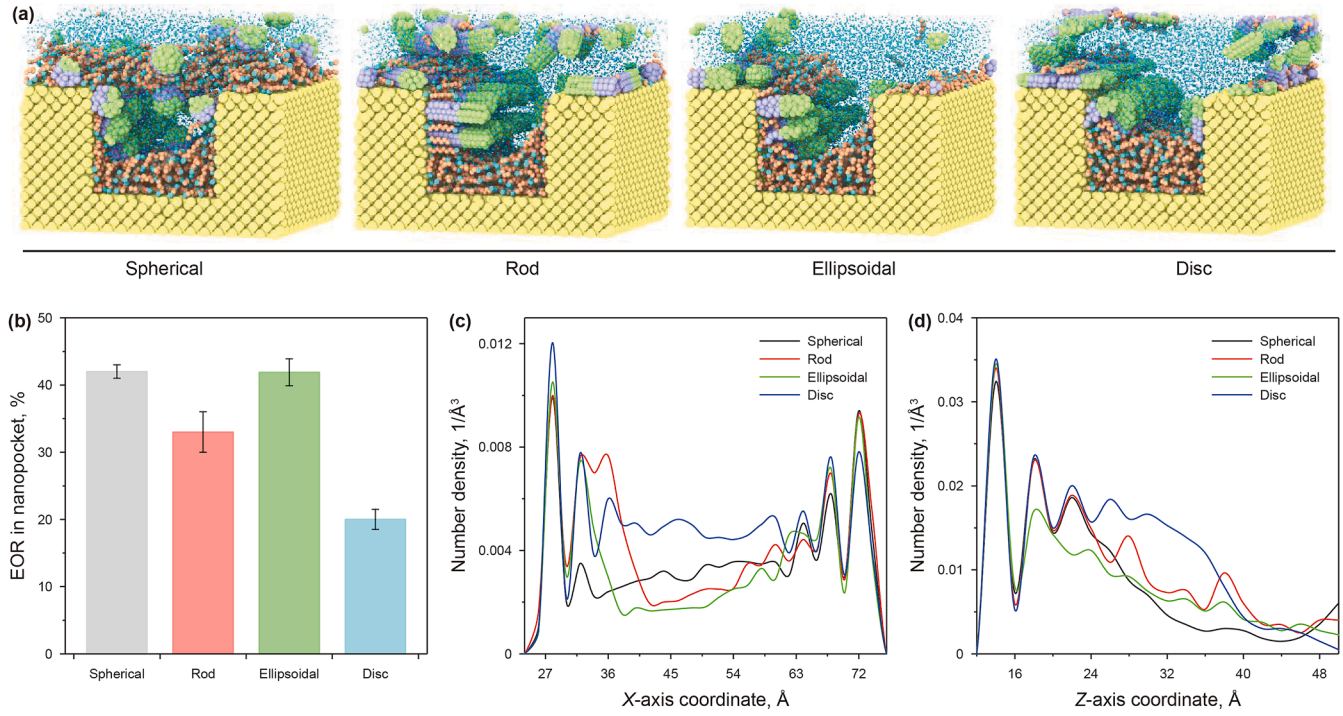

Fig. 2. Oil recovery performance of JNPs with different shapes. (**a**) Final system snapshots for different JNP geometries. (**b**) Oil recovery efficiency corresponding to each type of JNPs. (**c**) Spatial distribution of trapped oil molecules within the nanogroove after displacement, characterized by density profiles along the displacement direction (*X*-axis). (**d**) Density profiles along the groove depth (*Z*-axis), further illustrating the oil entrapment behavior.

different JNP shapes. It is worth noting that ellipsoidal JNPs not only extract the greatest amount of residual oil near the groove center but also penetrate deeper into oil-rich regions compared to other shapes, as illustrated in Fig. 2(d). In contrast, disc-shaped JNPs mainly interact with shallow oil layers, accounting for their inferior EOR performance. These findings clearly demonstrate that the unique motion behavior and shape-governed adsorption patterns of JNPs critically determine the underlying displacement mechanisms and resultant oil recovery efficiency, which will be further elaborated in the following sections.

3.2. Migration characteristics of JNPs with different shapes

3.2.1. The structure of adsorbed JNPs on the wall of the nanogroove

As discussed above, the adsorption of JNPs on the side of the nanogroove is crucial for the recovery of trapped oil. To further elucidate this relationship, it is essential to correlate the dynamic oil recovery, represented by the temporal evolution of oil molecule counts in Fig. 3(a), with the distribution and behavioral changes of JNPs adsorbed within the groove. To characterize the structural features of these adsorbed JNPs, three key indicators are employed: the number of adsorbed JNPs (N), the average centroid depth (D), and the average orientation angle (α). To be specific, the adsorbed JNP number N is the adsorption quantity of the JNPs on the wall of the nanogroove. The depth of the adsorbed NPs directly quantifies the migration of the NPs along the solid wall into the nanogroove, which is characterized by the average centroid depth D. As plotted in Fig. 3(b), a higher D value corresponds to deeper adsorption of JNPs on the solid wall inside the nanogroove. In addition, the orientation of JNPs on the solid wall has a direct impact on the alteration of local surface wettability. As JNPs adsorb with their polar ends oriented toward the liquid phase, the surface becomes more hydrophilic, effectively mimicking the characteristics of a water-like surface. The contribution of JNPs in local wettability alteration is reflected by the orientation angle α, which is defined as the angle between the side wall and the Janus interface, as sketched in Fig. 3(b).

The evolution of JNP adsorption structures, presented in Fig. 3(c), reveals that both the adsorption number N and adsorption depth D increase markedly during the displacement process, while the orientation angle α rapidly stabilizes. These trends are shape-dependent and result in distinct EOR outcomes. Specifically, spherical JNPs show a strong positive correlation between the changes in N and D. This implies that the newly adsorbed JNPs on the lateral surface promote deeper migration of pre-adsorbed ones. Interestingly, the EOR performance of spherical JNPs significantly declines at around 65 ns (Fig. 3(a)), coinciding with a local maximum in α (Fig. 3(c)). Structural snapshots show that a JNP positioned at the top of the lateral wall rotates during this stage due to the compression from an adjacent JNP positioned above it, exposing more of its nonpolar region to the surrounding liquid (highlighted with a red circle in Fig. S2). This action attracts nearby residual oil, forming an oil bridge above the groove (Fig. 2(a)) and consequently impeding further residual oil recovery by spherical JNPs. Unlike spherical JNPs, the increase in N of rod JNPs exerts little effect on D. Although these particles tend to adsorb deeper into the groove and consistently maintain a low α, their EOR efficiency remains significantly lower. This result is attributed to the elongated nonpolar segment of rod JNPs, which, upon adsorption to the lateral wall, effectively restricts the mobility of nearby oil molecules within a relatively large surrounding region. This confinement effect hampers oil displacement, thereby reducing the overall EOR efficiency. The velocity distribution of oil molecules at the end of the simulation further supports this finding, showing that rod JNPs immobilize nearby oil molecules upon adsorption (Fig. S3). Ellipsoidal JNPs provide the most stable EOR effect. Their adsorption characteristics combine the advantages of both spherical and rod JNPs, displaying a high correlation between N and D (similar to spherical JNPs) and promptly achieving a low α (consistent with rod JNPs). Conversely, disc JNPs display an exceedingly low EOR effect upon initial adsorption on the lateral surfaces, primarily due to their poor α, as depicted in Fig. S4. When adsorbed perpendicularly to the groove wall, these particles can only modify wettability over a limited area. The eventual improvement in EOR performance is primarily attributed to the accumulation of disc JNPs on the lateral surfaces over time.

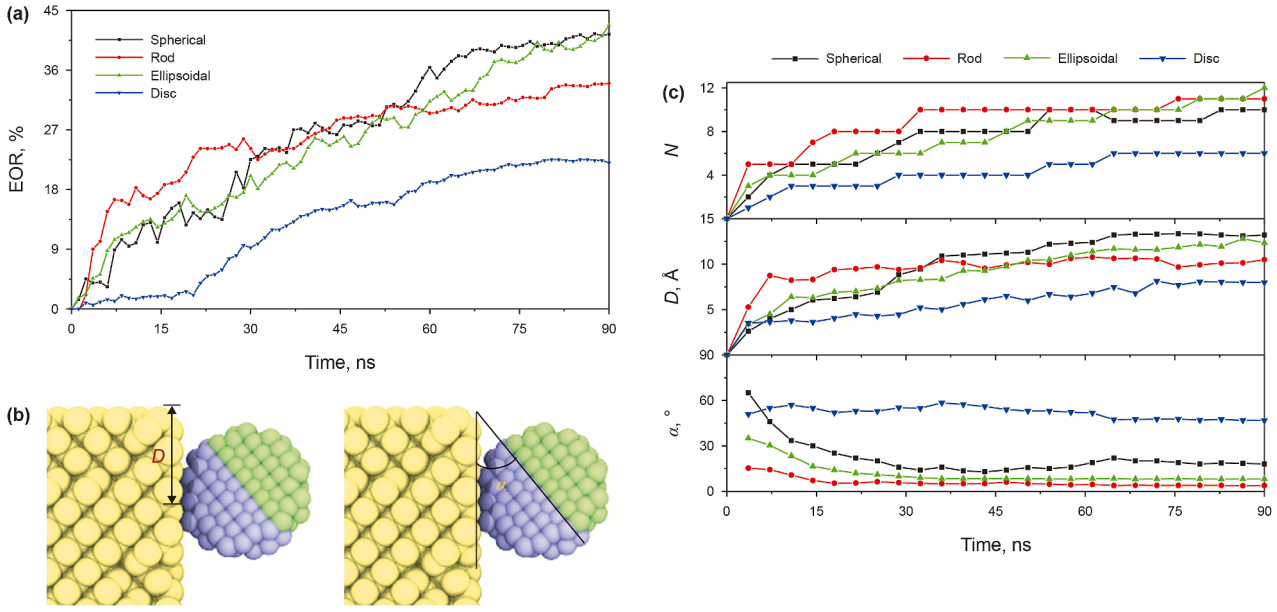

Fig. 3. EOR effect and the characterization of JNP adsorption structure. (**a**) The EOR effect inside the nanogroove during the displacement. (**b**) Schematic of adsorption depth and orientation of the JNP on the lateral surface. (**c**) Changes in three indicators of the JNPs migrating into the nanogroove, namely adsorption number (N), average centroid depth (D), and the adsorption orientation from top to bottom (α).

3.2.2. Motion pattern of adsorbed JNPs

JNPs exhibit distinct motion patterns depending on their shapes, which consequently dictate their adsorption structures along lateral surfaces. These motion patterns are fundamental in unraveling the underlying EOR mechanism. Fig. 4(a) illustrates a representative dynamic trajectory of a single JNP entering and stabilizing in a nano-groove. Among them, disc-shaped JNPs are initially pinned at the edge of the solid surface and subsequently reorient themselves while migrating along the lateral wall. In comparison, spherical, ellipsoidal, and rod JNPs first interact with residual oil adsorbed on the flat surface and then gradually slide along it toward the groove edge. Notably, all three of these JNP types tend to pause at the groove entrance, indicating the presence of a pinning effect, which has also been observed in previous experimental studies (Chang et al., 2016; Zhang et al., 2014). To confirm the existence and nature of this pinning effect, the potential of mean force (PMF) is calculated by employing umbrella sampling. This calculation quantifies the energy difference at diverse locations on the oil film surface for an individually adsorbed JNP, in the absence of external displacement forces. The displacement distance of the NP from its original position, along with the corresponding force from the harmonic potential, is recorded and processed via the weighted histogram analysis method (WHAM) algorithm (Beckmann et al., 2015; Choudhary et al., 2016). Given the symmetry of the system, calculations only cover the first half of the system in the *X*-direction. It is worth noting that the PMF profile of disc-shaped JNPs is not included due to its distinct interfacial behavior.

The resulting PMF profiles, shown in Fig. 4(b), reveal a pronounced energy minimum for all JNP types at the groove entrance, followed by a significant energy barrier that obstructs direct migration across the oil–water interface over the groove. Here, the energy barrier is defined as the difference in the potential of mean force between the energy minimum at the groove entrance and the subsequent maximum encountered as the JNP attempts to migrate into the groove interior. Among them, spherical JNPs exhibit the highest energy barrier, while rod-shaped JNPs face the lowest. These results align with their observed mobility: spherical JNPs remain most stably pinned at the groove edge, while rod-shaped JNPs are the least affected by the pinning effect.

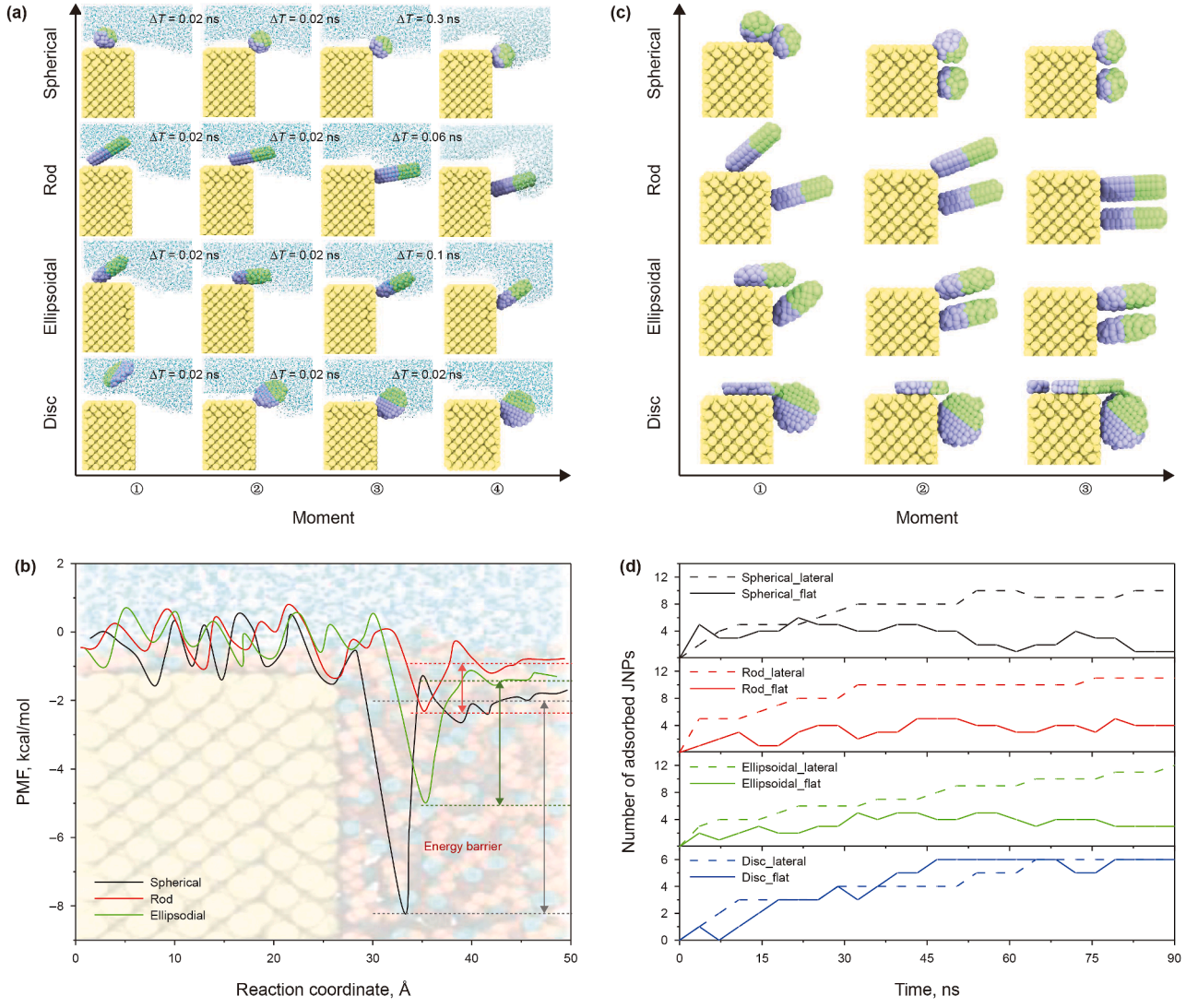

Fig. 4. Motion pattern of adsorbed JNPs. (**a**) The dynamics of individual JNPs with different shapes entering the nanogroove. Time intervals between moments are labeled in the figure. (**b**) The PMF of a JNP transporting from the left side of the surface to the middle of the nanogroove along the oil–water interface. (**c**) Typical processes in which a JNP located on the lateral surface is influenced by another JNP and subsequently migrates deeper into the groove. (**d**) The number variation of JNPs adsorbed on the flat and lateral surfaces during displacement.

Moreover, JNPs lingering at the edge can alter the local surface wettability due to their special surface wettability arrangement, and then adjust the local water flow direction (as plotted in Fig. S5). This redirection facilitates the propulsion of JNPs into the groove interior, where they reach a relatively stable configuration. The detachment times from the groove edge and final lateral positions for various JNP shapes (moment ④, Fig. 4(a)) align well with the varied pinning effects they encounter (Fig. 4(b)).

After clarifying the entry pathways of JNPs into the nanogroove, it is vital to examine their accumulation on the lateral surface. Fig. 4(c) documents a typical process wherein a JNP on the lateral surface is influenced by another JNP and subsequently penetrates deeper into the groove. For disc JNPs, as shown in Fig. S4, these particles adsorb onto the lateral wall with a consistent orientation angle and remain in a parallel alignment relative to neighboring JNPs. This parallel configuration minimizes steric and repulsive interactions by reducing overlapping contact zones. Additionally, disc JNPs moving across the flat surface apply continuous downward pressure on those already adsorbed on the lateral wall due to altered streamlines, making it difficult for the latter to reorient and deepen their position. In contrast, the other three shapes of JNPs exhibit cooperative dynamics on the lateral surface. For spherical JNPs, accumulation is primarily driven by direct collisions with incoming particles. In the case of rod and ellipsoidal JNPs, their migration into deeper lateral regions is induced by localized shifts in the water flow field triggered by adjacent JNPs. Importantly, continuous accumulation at the groove edge restricts the available space for new arrivals (refer to moment ③, Fig. 4(c)). This spatial limitation, coupled with varying degrees of the pinning effect at the surface edge, especially hinders the further layering of rod JNPs at the edge. Consequently, only a double-layer adsorption film forms under the current simulation conditions. Ellipsoidal JNPs, however, are less restricted by these factors and can accumulate on the lateral surface in a manner similar to spherical JNPs.

The distinct accumulation patterns for each JNP type are further confirmed by tracking adsorption dynamics on both the flat and lateral surfaces (Fig. 4(d)). For disc-shaped JNPs, the increase in lateral surface adsorption shows minimal correlation with changes on the flat surface. While the increase in the other three JNP types in lateral adsorption coincides with a decrease in surface-level adsorption. This indicates a redistribution mechanism wherein early-stage accumulation on the flat surface facilitates later migration to the lateral walls via collisions or flow-induced interactions. For spherical JNPs, this early accumulation is particularly prominent and forms the basis for their effective migration into the groove.

In summary, JNPs displace trapped oil primarily by adsorbing and accumulating on the lateral surfaces of nanogrooves, where they alter local wettability. Shape-dependent variations in surface recognition, local flow modulation, and pinning behavior give rise to diverse adsorption film architectures, which in turn directly influence EOR efficiency. Remarkably, the observed JNP dynamics in this study bear resemblance to the nucleation and growth of "climbing films" reported in previous experimental works (Luo et al., 2016). The findings thus offer novel nanoscale insights into the formation of adsorption films and elucidate how JNP shape governs their interaction with rough surfaces during the oil displacement process.

3.3. Effect of oil film thickness

Beyond the role of oil trapped within the nanogrooves, the influence of JNP geometry on oil film displacement becomes increasingly significant as the oil film thickens. As illustrated in Fig. 5(a), simulations were conducted across three representative oil film thicknesses to assess the overall EOR performance of various JNP shapes, considering both the oil film and the residual oil trapped in the groove. It is apparent that the EOR effect of spherical JNPs diminishes dramatically with increasing oil film thickness, while in other cases, its impact is relatively moderate. This discrepancy can be attributed primarily to the limited ability of spherical JNPs to penetrate and mobilize thicker oil films, as confirmed by the post-simulation snapshots in Fig. S6. Moreover, this simulation result implies that for spherical JNPs of fixed size, there exists a critical planar oil film thickness beyond which their effectiveness in mobilizing surface oil films becomes negligible. In contrast, other JNPs, which possess high interfacial instability, follow a mode known as "aggregation and flipping" to continually remove oil from the surface. Take ellipsoidal JNPs as a representative example (with comparable processes for disc and rod JNPs depicted in Fig. S7), the particles initially adsorb at the oil–water interface in a range of orientations (moment ①, Fig. 5(b)). During the sliding, JNPs are then subjected to different magnitudes and directions of thrust, leading some of them to gradually aggregate (moment ②, Fig. 5(b). These aggregates, driven by the surrounding water flow, undergo flipping motions that cause them to detach from the oil film surface (moment ④, Fig. 5(b)). Subsequently, free JNPs in the bulk phase capture the detached aggregates, which load with residual oil, leading to the spontaneous formation of Pickering emulsions (moment ⑤, Fig. 5(b)).

Furthermore, to evaluate the impact of different JNPs on oil displacement in the nanogroove under various oil film thicknesses, the corresponding adsorption structures on the lateral surface are characterized in Fig. 5(c). Generally, the quality of all JNP adsorption structures degrades as the oil film thickness increases, with spherical JNPs notably unable to enter the nanogroove under thick oil film conditions. Yet, for rod and ellipsoid JNPs, their adsorption structures in the nanogroove are only mildly affected when the oil film thickness reaches 10 Å. This behavior is intrinsically linked to their long nonpolar ends, whose length approaches the oil film thickness (rod JNPs and ellipsoid JNPs are 10.2 and 8.9 Å, respectively). These extended nonpolar ends allow partial penetration into the film, enabling the JNPs to adsorb directly onto the solid surface via transient oil–water interface fluctuations. Once adsorbed, they gradually migrate into the nanogroove and accumulate over time.

Under thicker oil film conditions, an initial portion of the oil is displaced through the aforementioned "aggregation and flipping" mechanism. Subsequent free JNPs then begin to adsorb onto the exposed surface. However, given a fixed total number of injected JNPs, a thicker oil film reduces the number of particles available for surface adsorption. As a result, the coverage area of the adsorption layer diminishes, limiting the extent of trapped oil extraction within the nanogroove. This highlights two potential strategies for improving recovery performance under thick oil film conditions: (1) engineering JNPs with longer nonpolar tails to enhance surface penetration, and (2) increasing the overall JNP injection concentration to ensure adequate surface coverage.

Besides, the quantity of rod and ellipsoidal JNPs that could involve in the displacement of nanogrooves is tracked respectively at an oil film thickness of 15 Å. Temporal variations in JNP counts, along with the number of remaining oil molecules on the flat surface, are presented in Fig. S8. It is found that ellipsoidal JNPs exhibit higher efficiency in displacing the surface oil film compared to rod-shaped JNPs, meaning that fewer ellipsoidal particles are needed to remove the same amount of oil from the flat lateral surface. Consequently, more ellipsoidal JNPs remain unadsorbed and available to penetrate deeper into the groove, where they can more effectively mobilize and displace the trapped

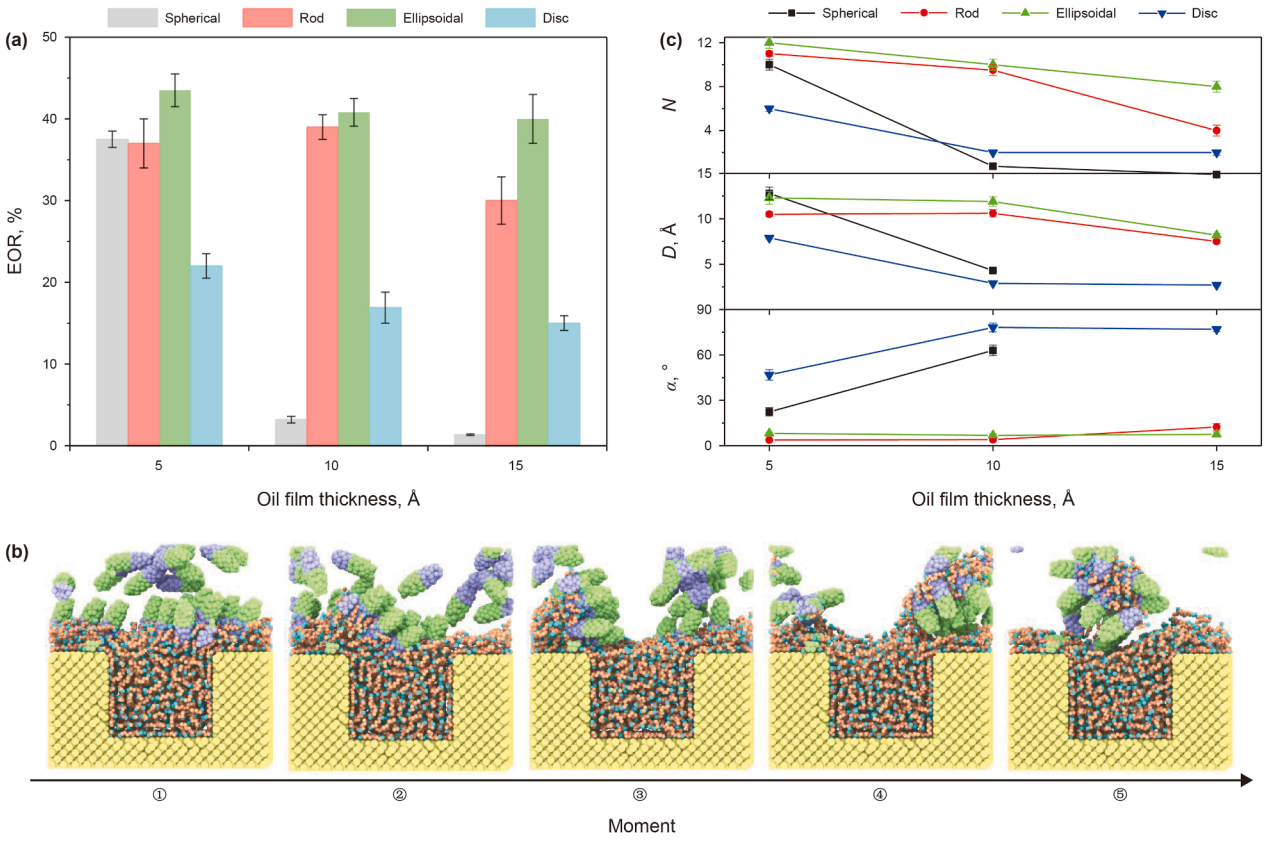

Fig. 5. Effect of oil film thickness in displacing trapped oil by varied JNPs. (**a**) EOR effect of JNPs with different shapes under varying oil film thickness. (**b**) The representative process of ellipsoidal JNPs displacing the surface oil film. (**c**) Characterization of JNP adsorption structures formed by types of JNPs after displacements under three oil film thicknesses.

oil clusters in confined regions. This favorable distribution leads to the formation of more effective adsorption configurations, as shown in Fig. 5(c), and results in superior overall oil recovery performance, particularly under conditions of high oil film thickness, as demonstrated in Fig. 5(a).

3.4. Discussion

The above findings elucidate the advantages and underlying mechanisms by which ellipsoidal JNPs mobilize residual oil under complex pore-scale conditions. The superior performance of such anisotropic NPs has also been recognized in experimental studies, where ellipsoidal cellulose nanocrystals and rutile ellipsoidal TiO_2 NPs have demonstrated outstanding EOR capabilities, primarily attributed to their favorable transport behavior and interfacial properties (Aadland et al., 2020; Hu et al., 2016). Our simulation results further reinforce the notion that NP shape anisotropy significantly influences the behavior and efficacy of NPs during oil displacement. Despite growing interest in non-spherical NPs, there remains a notable lack of systematic studies that directly compare the EOR performance and mechanisms of NPs with different geometries under consistent fluid–solid interfacial conditions, particularly for Janus-type systems. Previous research has predominantly focused on spherical inorganic NPs, while emerging evidence suggests that transitioning from spherical to disc-like morphologies can enhance NP dispersion, reduce interfacial tension (Zaid et al., 2014). Notably, flexible disc-shaped materials such as smart black nanocards have been shown to significantly enhance oil recovery through the generation of structural disjoining pressure rather than interfacial tension reduction (Geng et al., 2024; Li et al., 2022). Nanocards have also been reported to exhibit excellent foam-stabilizing capabilities (Raj et al., 2020). In contrast, the disc-like JNPs investigated in this study were modeled as rigid structures and specifically evaluated in the context of displacing thin adsorbed oil films on solid surfaces, a process that is difficult to isolate in experiments, which typically capture only the overall recovery performance. Under such conditions, disc-like JNPs were found to be less effective than their spherical counterparts. These findings suggest that the effectiveness of NP geometry is strongly system-dependent, and its governing mechanisms can vary with both particle rigidity and the fluid–rock environment. Future research should aim to systematically elucidate the dominant oil displacement mechanisms and application scenarios associated with NPs of different shapes to further advance targeted EOR strategies.

Besides, while the study provides fundamental insights into the shape-dependent mechanisms of JNP-assisted oil displacement, several limitations should be acknowledged. Firstly, the nanoparticles modeled in our simulations are significantly smaller than those typically used in experimental or field-scale applications, a necessary compromise due to the computational constraints of molecular dynamics simulations. Secondly, the oil phase used in this study consists solely of hexane, which serves as a simplified model to isolate and compare the behavior of different nanoparticle morphologies. In reality, crude oil contains a wide range of polar components, such as pyridines and asphaltenes, which are known to preferentially adsorb at interfaces and solid surfaces, thereby altering fluid properties and potentially hindering displacement efficiency. Additionally, the simulations are conducted in a single, idealized groove structure, which does not fully

capture the complexity and heterogeneity of real reservoir pore networks. Thus, future work will aim to incorporate more representative oil compositions to better reflect the chemical complexity of crude oil systems. It will also be necessary to employ coarse-grained simulation methods such as dissipative particle dynamics (DPD) to model JNPs of more realistic sizes and to evaluate potential size-dependent behavior. Furthermore, further studies will focus on exploring the displacement dynamics and EOR effectiveness of various JNP morphologies in residual oil systems within complex multipores, with the goal of extending mechanistic understanding to more realistic porous environments.

4. Conclusions

The effects and underlying mechanisms of trapped oil displacement from rough surfaces by JNPs of varying shapes have been elucidated through MD simulations. The results demonstrate that in nanogrooves covered with a thin oil film, ellipsoidal and spherical JNPs exhibit superior performance in displacing trapped oil. A key observation is that the shape of JNPs plays a decisive role in forming distinct adsorption structures on the lateral surface of the nanogroove, which markedly modify the local surface wettability alteration and resulting oil displacement effect. This role originates from the unique motion patterns exhibited by distinct JNPs. Specifically, disc-shaped JNPs tend to be captured at the groove edges, and their unfavorable orientations limit their ability to penetrate deeper into the groove. In contrast, ellipsoidal, spherical, and rod-like JNPs are capable of entering the grooves via surface adsorption followed by lateral sliding. Among them, ellipsoidal and spherical JNPs experience stronger pinning effects at the groove entrance, enabling sustained accumulation along the sidewalls. Additionally, the extraction of trapped oil inside the nanogroove by JNPs is impeded by a thick oil film. While rod and ellipsoidal JNPs can effectively desorb this surface oil film through the “aggregation and flipping” mechanism. Notably, ellipsoidal JNPs consistently achieve the highest oil recovery efficiency across various scenarios. These results mark the first nanoscale comprehension of trapped oil displacement by JNPs of different shapes. Such insights greatly contribute to the design and selection of optimally performing JNPs for EOR applications.

CRediT authorship contribution statement

Yuan-Hao Chang: Writing – original draft, Conceptualization. **Rui Ma:** Software, Methodology. **Bo Wang:** Software. **Han-Zhou Li:** Writing – review & editing. **Fan-Hua Zeng:** Supervision. **Jian-Ying He:** Writing – review & editing, Validation.

Declaration of interests

The authors declare that they have no known competing financial interests or personal relationships that could have appeared to influence the work reported in this paper.

Acknowledgements

This work was financially supported by the Research Council of Norway (Grant No. 234626). The supercomputer CPU hours were provided by the Norwegian Metacenter for Computational Science (Project ID: NN9110K and NN9391K).

Supplementary data

Supplementary data to this article can be found online at https://doi.org/10.1016/j.petsci.2025.12.024.

References

Aadland, R.C., Akarri, S., Heggset, E.B., Syverud, K., Torsæter, O., 2020. A core flood and microfluidics investigation of nanocellulose as a chemical additive to water flooding for EOR. Nanomaterials 10 (7), 1296. https://doi.org/10.3390/nano10071296.

Ahmadi, Y., Eshraghi, S.E., Bahrami, P., Hasanbeygi, M., Kazemzadeh, Y., Vahedian, A., 2015. Comprehensive water–alternating-gas (WAG) injection study to evaluate the most effective method based on heavy oil recovery and asphaltene precipitation tests. J. Petrol. Sci. Eng. 133, 123–129. https://doi.org/10.1016/j.petrol.2015.05.003.

Almahfood, M., Bai, B., 2018. The synergistic effects of nanoparticle-surfactant nanofluids in EOR applications. J. Petrol. Sci. Eng. 171, 196–210. https://doi.org/10.1016/j.petrol.2018.07.030.

Bai, B., 2008. Overview: eOR/IOR. J. Petrol. Technol. 60 (1), 42. https://doi.org/10.2118/0108-0042-JPT.

Beckmann, A., Xiao, S., Müller, J.P., Mercadante, D., Nüchter, T., Kröger, N., Langhojer, F., Petrich, W., Holstein, T.W., Benoit, M., 2015. A fast recoiling silk-like elastomer facilitates nanosecond nematocyst discharge. BMC Biol. 13, 1–16. https://doi.org/10.1186/s12915-014-0113-1.

Betancur, S., Carmona, J.C., Nassar, N.N., Franco, C.A., Cortés, F.B., 2016. Role of particle size and surface acidity of silica gel nanoparticles in inhibition of formation damage by asphaltene in oil reservoirs. Ind. Eng. Chem. Res. 55 (21), 6122–6132. https://doi.org/10.1021/acs.iecr.6b01187.

Chang, B., Zhou, Q., Ras, R.H., Shah, A., Wu, Z., Hjort, K., 2016. Sliding droplets on hydrophilic/superhydrophobic patterned surfaces for liquid deposition. Appl. Phys. Lett. 108 (15), 154102. https://doi.org/10.1063/1.4947008.

Chang, Y., Xiao, S., Fu, Y., Wang, X., Zhang, Z., He, J., 2021. Nanomechanical characteristics of trapped oil droplets with nanoparticles: A molecular dynamics simulation. J. Petrol. Sci. Eng., 108649 https://doi.org/10.1016/j.petrol.2021.108649.

Chang, Y., Xiao, S., Ma, R., Zhang, Z., He, J., 2022. Atomistic insight into oil displacement on rough surface by Janus nanoparticles. Energy 245, 123264. https://doi.org/10.1016/j.energy.2022.123264.

Choudhary, N., Das, S., Roy, S., Kumar, R., 2016. Effect of polyvinylpyrrolidone at methane hydrate-liquid water interface. Application in flow assurance and natural gas hydrate exploitation. Fuel 186, 613–622. https://doi.org/10.1016/j.fuel.2016.09.004.

Gao, H., Hu, J., Chi, M., Fan, J., Zhang, T., Xie, W., Ituen, E., Sun, S., Li, C., Hu, S., 2025. Design and synthesis of temperature-responsive Janus nanoparticles with high salt tolerant for enhanced heavy oil recovery. Geoenergy Sci. Eng. 244, 213433. https://doi.org/10.1016/j.geoen.2024.213433.

Geng, X., Ding, B., Guan, B., Sun, H., Zan, J., Qu, M., Liang, T., Li, H., Hu, S., 2024. New insight of nanosheet enhanced oil recovery modeling: Structural disjoining pressure and profile control technique simulation. Energies 17 (23), 5897. https://doi.org/10.3390/en17235897.

Giraldo, L.J., Gallego, J., Villegas, J.P., Franco, C.A., Cortés, F.B., 2019. Enhanced waterflooding with NiO/SiO_2 0-D Janus nanoparticles at low concentration. J. Petrol. Sci. Eng. 174, 40–48. https://doi.org/10.1016/j.petrol.2018.11.007.

Haruna, M.A., Gardy, J., Yao, G., Hu, Z., Hondow, N., Wen, D., 2020. Nanoparticle modified polyacrylamide for enhanced oil recovery at harsh conditions. Fuel 268, 117186. https://doi.org/10.1016/j.fuel.2020.117186.

Hoover, W.G., 1985. Canonical dynamics: Equilibrium phase-space distributions. Phys. Rev. 31 (3), 1695. https://doi.org/10.1103/PhysRevA.31.1695.

Hu, Z., Azmi, S.M., Raza, G., Glover, P.W., Wen, D., 2016. Nanoparticle-assisted water-flooding in Berea sandstones. Energy Fuels. 30 (4), 2791–2804. https://doi.org/10.1021/acs.energyfuels.6b00051.

Jia, H., Dai, J., Miao, L., Wei, X., Tang, H., Huang, P., Jia, H., He, J., Lv, K., Liu, D., 2021a. Potential application of novel amphiphilic Janus-SiO_2 nanoparticles stabilized O/W/O emulsion for enhanced oil recovery. Colloids Surf. A Physicochem. Eng. Asp. 622, 126658. https://doi.org/10.1016/j.colsurfa.2021.126658.

Jia, X., Luo, J., Wang, P., He, M., Wang, Y., Peiwen, X., Jiang, B., 2021b. Synthesis of dumbbell-like SiO_2 nanoparticles with amphiphilic properties in aqueous phase. Chin. J. Inorg. Chem. 37 (4), 653–660. https://doi.org/10.11862/CJIC.2021.061.

Li, H., Wang, C., Li, B., Wen, X., Li, J., Tian, L., 2022. Experimental investigation on the imbibition behavior of nanofluids in the tight oil and gas reservoir through the application of nuclear magnetic resonance method. Energies 16 (1), 454. https://doi.org/10.3390/en16010454.

Liu, L., Tang, L., Yan, X., Zuo, T., Zheng, X., Deng, J., Shi, W., 2025. Potential application of novel amphiphilic Janus SiO_2 nanoparticles for stable pickering emulsion and enhance oil recovery. Surf. Interfaces 64, 106467. https://doi.org/10.1016/j.surfin.2025.106467.

Luo, D., Wang, F., Zhu, J., Cao, F., Liu, Y., Li, X., Willson, R.C., Yang, Z., Chu, C.-W., Ren, Z., 2016. Nanofluid of graphene-based amphiphilic Janus nanosheets for tertiary or enhanced oil recovery: High performance at low concentration. Proc. Natl. Acad. Sci. 113 (28), 7711–7716. https://doi.org/10.1073/pnas.1608135113.

Luu, X.C., Striolo, A., 2014. Ellipsoidal Janus nanoparticles assembled at spherical oil/water interfaces. J. Phys. Chem. B 118 (47), 13737–13743. https://doi.org/10.1021/jp5085422.

Lyons, W.C., Plisga, G.J., 2011. Standard Handbook of Petroleum and Natural Gas Engineering. Elsevier.
Martin, M.G., Siepmann, J.I., 1998. Transferable potentials for phase equilibria. 1. United-atom description of *n*-alkanes. J. Phys. Chem. B 102 (14), 2569–2577. https://doi.org/10.1021/jp972543+.
Molinero, V., Moore, E.B., 2009. Water modeled as an intermediate element between carbon and silicon. J. Phys. Chem. B 113 (13), 4008–4016. https://doi.org/10.1021/jp805227c.
Newell, R., Raimi, D., Aldana, G., 2019. Global energy outlook 2019: The next generation of energy. Resourc. Fut. 1 (8), 1–37.
Nosé, S., 1984. A unified formulation of the constant temperature molecular dynamics methods. J. Chem. Phys. 81 (1), 511–519. https://doi.org/10.1063/1.447334.
Olajire, A.A., 2014. Review of ASP EOR (alkaline surfactant polymer enhanced oil recovery) technology in the petroleum industry: Prospects and challenges. Energy 77, 963–982. https://doi.org/10.1016/j.energy.2014.09.005.
Plimpton, S., 1995. Fast parallel algorithms for short-range molecular dynamics. J. Comput. Phys. 117 (1), 1–19. https://doi.org/10.1006/jcph.1995.1039.
Raj, I., Liang, T., Qu, M., Xiao, L., Hou, J., Xian, C., 2020. An experimental investigation of MoS_2 nanosheets stabilized foams for enhanced oil recovery application. Colloids Surf. A Physicochem. Eng. Asp. 606, 125420. https://doi.org/10.1016/j.colsurfa.2020.125420.
Raj, I., Qu, M., Xiao, L., Hou, J., Li, Y., Liang, T., Yang, T., Zhao, M., 2019. Ultralow concentration of molybdenum disulfide nanosheets for enhanced oil recovery. Fuel 251, 514–522. https://doi.org/10.1016/j.fuel.2019.04.078.
Richards, P.W., Frankham, R., Walsh, R., 1996. The Tropical Rain Forest: An Ecological Study. Cambridge University Press.
Rosales, S., Machín, I., Sánchez, M., Rivas, G., Ruette, F., 2006. Theoretical modeling of molecular interactions of iron with asphaltenes from heavy crude oil. J. Mol. Catal. Chem. 246 (1–2), 146–153. https://doi.org/10.1016/j.molcata.2005.10.027.
Shi, F., Wu, J., Zhao, B., Zhao, Y., Yu, X., 2019. Structural characterization and oil displacement performance of Janus micro-nanocapsules. J. Silic. 11. https://doi.org/10.14062/j.issn.0454-5648.2019.11.20.
Stukowski, A., 2009. Visualization and analysis of atomistic simulation data with OVITO–the open visualization tool. Model. Simulat. Mater. Sci. Eng. 18 (1), 015012. https://doi.org/10.1088/0965-0393/18/1/015012.
Sun, X., Dong, M., Zhang, Y., Maini, B.B., 2015. Enhanced heavy oil recovery in thin reservoirs using foamy oil-assisted methane huff-n-puff method. Fuel 159, 962–973. https://doi.org/10.1016/j.fuel.2015.07.056.
Sun, X., Zhang, Y., Chen, G., Gai, Z., 2017. Application of nanoparticles in enhanced oil recovery: A critical review of recent progress. Energies 10 (3), 345. https://doi.org/10.3390/en10030345.
Tang, S., Sun, Z., Dong, Y., Zhu, Y., Hu, H., Wang, R., Liao, H., Dai, Q., 2024. Preparation of amphiphilic Janus-SiO_2 nanoparticles and evaluation of the oil displacement effect. ACS Omega 9 (5), 5838–5845. https://doi.org/10.1021/acsomega.3c08979.
Tohidi, Z., Teimouri, A., Jafari, A., Gharibshahi, R., Omidkhah, M.R., 2022. Application of Janus nanoparticles in enhanced oil recovery processes: Current status and future opportunities. J. Petrol. Sci. Eng. 208, 109602. https://doi.org/10.1016/j.petrol.2021.109602.
Wang, X., Xiao, S., Zhang, Z., He, J., 2019. Transportation of Janus nanoparticles in confined nanochannels: A molecular dynamics simulation. Environ. Sci. Nano 6 (9), 2810–2819. https://doi.org/10.1039/c9en00314b.
Wang, X., Zhang, Z., Zhang, J., He, J., 2020. Insight into the pressure-induced displacement mechanism for selecting efficient nanofluids in various capillaries. Environ. Sci. Nano 7 (9), 2785–2794.
Wu, G., Lang, W., Li, X., Hou, Z., Zhao, X., Tian, Z., Song, J., Jia, H., 2024. Potential application of novel Janus amphiphilic nanoparticles to improve the viscoelasticity of polymer solution for enhanced oil recovery. J. Dispersion Sci. Technol. 1–10. https://doi.org/10.1080/01932691.2024.2377742.
Wu, H., Gao, K., Lu, Y., Meng, Z., Gou, C., Li, Z., Yang, M., Qu, M., Liu, T., Hou, J., 2020a. Silica-based amphiphilic Janus nanofluid with improved interfacial properties for enhanced oil recovery. Colloids Surf. A Physicochem. Eng. Asp. 586, 124162. https://doi.org/10.1016/j.colsurfa.2019.124162.
Wu, J., Shi, F., Zhao, Y., Zhang, M., Cai, L., 2020b. Research progress of functional nano oil displacement agents. J. Northeast Petrol. Univ. https://doi.org/10.3969/j.issn.2095-4107.2020.05.001 (in Chinese).
Zaid, H.M., Radzi, N.S.A., Latiff, N.R.A., Shafie, A., 2014. Effect of morphology of aluminium oxide nanoparticles on viscosity and interfacial tension (IFT) and the recovery efficiency in enhanced oil recovery (EOR). In: Proceedings AIP Conference Proceedings. American Institute of Physics. https://doi.org/10.1063/1.4898545.
Zang, L., Hu, M., Cao, J., Cheng, Y., Li, P., Guo, J., Zhang, H., 2024. Design of Janus nanoparticles for mobility control in heterogeneous reservoirs. ACS Omega 9 (14), 16536–16546. https://doi.org/10.1021/acsomega.4c00317.
Zhang, P., Liu, H., Meng, J., Yang, G., Liu, X., Wang, S., Jiang, L., 2014. Grooved organogel surfaces towards anisotropic sliding of water droplets. Adv. Mater. 26 (19), 3131–3135. https://doi.org/10.1002/adma.201305914.